Soft Matter

Accepted Manuscript

ROYAL SOCIETY OF CHEMISTRY

www.rsc.org/softmatter

Journal Name

RSCPublishing

ARTICLE

Modelling of noble anesthetic gases and high hydrostatic pressure effects in lipid bilayers

Cite this: DOI: 10.1039/x0xx00000x

Received ooth January 2012,
Accepted ooth January 2012

DOI: 10.1039/x0xx00000x

www.rsc.org/

Yevgeny Moskovitz* and Hui Yang

Department of Chemistry, Middle Tennessee State University, Murfreesboro, TN 37130, USA

Keywords: *molecular dynamics; lipid bilayer; general anesthesia; pressure reversal; noble gases; high pressure nervous syndrome; transmembrane ionic current; hyperbaric breathing mixture; deep diving.*

Our objective was to study molecular processes that might be responsible for inert gas narcosis and high-pressure nervous syndrome. The classical molecular dynamics trajectories (200 ns-long) of dioleoylphosphatidylcholine (DOPC) bilayers simulated by the Berger force field were evaluated for water and the atomic distribution of noble gases around DOPC molecules at a pressure range of 1 - 1000 bar and temperature of 310 Kelvin. Xenon and argon have been tested as model gases for general anesthetics, and neon has been investigated for distortions that are potentially responsible for neurological tremor at hyperbaric conditions. The analysis of stacked radial pair distribution functions of DOPC headgroup atoms revealed the explicit solvation potential of gas molecules, which correlates with their dimensions. The orientational dynamics of water molecules at the biomolecular interface should be considered as an influential factor; while excessive solvation effects appearing in the lumen of membrane-embedded ion channels could be a possible cause of

*Corresponding author: Department of Chemistry, Scientific Computing Research Unit, University of Cape Town, Rondebosch 7701, Western Cape, South Africa. *e-mail*: klw54cp@gmail.com

Journal Name RSCPublishing

ARTICLE

inert gas narcosis. All the noble gases tested exhibit similar patterns of the order parameter for both DOPC acyl chains, which is opposite to the patterns found for the order parameter curve at high hydrostatic pressures in intact bilayers. This finding supports the 'critical volume' hypothesis of anesthesia pressure reversal. The irregular lipid headgroup-water boundary observed in DOPC bilayers saturated with neon in the pressure range of 1 - 100 bar could be associated with the possible manifestation of neurological tremor at the atomic scale. The non-immobilizer neon also demonstrated the highest momentum impact on the normal component of the DOPC diffusion coefficient representing monolayers undulations rate, which indicates enhanced diffusivity, rather than atom size, as the key factor.

Introduction

The limits of physiological adaptation by living organisms to hyperbaric aquatic environments is largely an unsolved mystery, despite the rapidly growing body of theoretical and experimental knowledge about the effects of hyperbaric gases and hydrostatic pressure *per se* at all meaningful scales, from biomolecular complexes to entire organisms[1,2]. Among the broad spectrum of potentially harmful factors, such as hyperbaric oxygen, and especially in hypercapnic conditions, the most intriguing aspect is the problem of the narcotic potency of noble gases and also their relevance to medical applications[3]. If one further considers the diminishing effect of anesthesia as hydrostatic pressure increases, and the development of so-called high pressure nervous syndrome (HPNS), the possibility emerges that these phenomena are somehow interdependent and could be explored on some common basis[4].

The physical conditions determining inert gas narcosis (IGN) and its symptoms have been well described in many sources[3,5]. According to the most common definition, gases become narcotic when their partial pressure exceeds 4 bar, depending on collateral circumstances such as body fat fraction, CO_2 retention, temperature etc. The narcotic potency of noble gases directly correlates with their atomic weight and the size of the respective gas atoms. According to these properties, the anesthetic row would be as follows: Xe(54)>Kr(36)>Ar(18)>Ne(10)>He(2) (the atomic number is in parentheses). Xenon, the most potent anesthetic, reveals its effect even at normobaric pressure, which makes it an intriguing medical agent for its neuroprotective characteristics[6]. On the other hand, neon's narcotic potency is questionable, while helium has no reported narcotic tendency – at least in physiologically reasonable pressure ranges. In this regard, it would be logical to assume the existence of a dynamic narcotic threshold moving towards the lighter gases (i.e. smaller gas atoms) as the concentration of solvated gas increases along with hydrostatic pressure, while pressure *per se* and gases below the threshold would have an antagonistic neutralizing effect on anesthetic sedative action.

Unlike anesthesia, HPNS is characterized by increased excitability of the central nervous system (CNS) and cognitive impairment involving memory disorders. HPNS has been reported in humans at pressures >10 bar and is mostly connected with the compressive effect of helium in a breathing mixture; its severity additionally depends on the rate of compression[7]. In species that breathe in a gaseous environment, it is hard to discriminate between the effects of saturated gases, especially helium (cf. helium tremors – the other term describing HPNS), and the effects of high hydrostatic pressure (HHP) *per se*. Little is known of the neurological effects of pressure among free-diving mammals that are well adapted to extremely high pressures and are able to withstand these without visible harm[8]. Worth noting is that the current no-limits apnea (NLT) free diving record for a human being is 214 meters of seawater (msw), a depth of 701 msw has been achieved at dry pressurized habitat while breathing a hydrogen-helium-oxygen (hydreliox) gas mixture[9,1]. As neurological data for totally immersed dogs that breathed pressure-oxygenated salt solutions at 8 bar are also not available[10], the hyperbaric effects of helium are frequently reported as a pressure effect (this might be a misleading simplification).

The theories of gaseous anesthetics originated at the end of the 19th century, and suggested different focuses and mechanisms for anesthetic agents; Meyer-Overton indicated the lipid phases as the main loci, and Paulling discussed hydrate formation at the water-

lipid boundary[11]. Transmembrane proteins, according to the current level of knowledge, are the most important target for general anesthesia; however, simple chemical consideration of inert gases and a considerable body of experimental evidence have shown that general gaseous anesthetics must have pluripotent activity, targeting lipids and trans-membrane proteins, and implicitly affecting water molecules at the lipid-solvent interface. Therefore, more highly ordered interfacial water is sometimes referred to as Miller's 'iceberg' hypothesis, as an alternative to Paulling's theory[12]. Recent experimental work on the biological effect of xenon demonstrated a non-competitive inhibition of the effect of glutamate receptor NMDA on transmembrane potassium channels such as TREK and TASK[6]. Crystallographic experiments have also been performed on proteins at a wide range of gas pressures, and it has been demonstrated that the anesthetic effect may be attributed to the gas affinity for carbon atoms located within highly hydrophobic cavities in protein cores[13].

The molecular mechanisms responsible for narcosis and HPNS are obviously different, in that a hydrostatic pressure increase apparently straightens molecular machinery affected by IGN, but it simultaneously initiates a pathological response in the deformed signal transduction chain, causing HPNS as the concentration of solvated He increases. Also, contrary effects on glutamate NMDA receptors have been reported for xenon and hydrostatic pressure variations[14]. However, it appears that the most fundamental level for IGN activity as well as for HPNS effects is the lipid molecule itself, for it 'anchors' to much more complicated transmembrane protein complexes. Understanding the molecular responses of lipids to IGN and high pressure might shed light on the processes taking place in transmembrane ion channels. For example, a high fraction of unsaturated lipids in the cell membranes of deep inhabitants – one of the most important adaptive factors to high pressures – has been reported, which makes them by definition a natural object for high-pressure biology research[15]. Lipids have been thoroughly explored by many experimental and computational tools, while new force field parameters have been continually tested. The present research focuses on the conformational changes of lipids owing to the presence of noble gases, and their reduction by HHP and associated processes studied by computational means.

Molecular dynamics (MD) simulations have been intensively used to study the dynamic and structural properties of biomolecules at all structural levels, and at time scales of up to hundreds of nanoseconds and even microseconds; continual increases in computer capacity promise to exceed these current, and still rarely attainable, values. The quality of MD output is very dependent on specific potential functions known as force fields (FF), which describe intra- and intermolecular interactions of simulated molecules. The basic criterion of the validation of an empirical FF is its ability to reproduce *ab initio* data and experimental observables such as lipid order parameter, area per lipid, atomic and electron density profiles, headgroup orientations etc. The few major non-polarizable FFs currently available for lipids have been extensively optimized by quantum mechanics – most commonly these FFs are applied CHARMM27, Berger, and GROMOS[16,17]. For exploring lipid hydration characteristics, a new polarizable FF-CHARMM charge equilibration (CHEQ) was developed for which polarization is accounted for via the migration of charge density between atomic species within a given molecule. This FF is able to present improved data on the degree of solvation of the lipid interior[18].

The aforementioned non-polarizable Berger FF applied in this research, although deviating from experiments (e.g., regarding partition coefficients for ethanol[19]), images mostly qualitative changes in the bilayer that might be associated with IGN and HPNS. It was chosen to be applicable because it was especially able to reproduce lipid order parameters with high precision, and natural lipid packing at zero surface tension. The gas distribution along bilayers at different pressure values, as the most important parameters possibly relevant for inducing IGN and HPNS, was calculated by means of a series of radial distribution functions (RDF). The lipid order parameter was estimated for both acyl chains of the DOPC molecule as a function of ambient hydrostatic pressure. The water distribution was analyzed in the headgroup atoms, as well as the bilayer thickness and area.

Methods

The fully hydrated lipid bilayer consisting of 288 pre-equilibrated DOPC molecules in a cubic box was solvated with 11 208 water molecules at a starting point. The extended simple point charge (SPC) water model was used and periodic boundary conditions (PBC) were employed. In all deployed systems, the gas concentration was constant, with the aim of ascertaining pure pressure effects and assuming a completely saturated bilayer; 888 solvent molecules were randomly replaced by gas atoms. The bilayer exposed to pure solvent was tested as a reference system. The gas

atoms were treated as simple Lennard-Jones (LJ) sites with interaction parameters as follows: for xenon ε=1.900 kJ mol^{-1} σ=0.406 nm; for argon ε=0.979 kJ mol^{-1} σ=0.340 nm; and for neon ε=0.289 kJ mol^{-1} σ=0.278 nm. The same parameters were used in previous simulations of gases in lipid bilayers[20,21].

The GROMACS 4.5.4 package was used for the simulation setup and analysis[22]. The Kraken Cray XT5 supercomputer at the Oak Ridge National Laboratory was used for our calculations. Each simulation lasted for at least 200 ns, divided by 25 ns sampling subtrajectories. The pressure range tested was 1, 25, 50, 100, 200, 350, 500 and 1000 bar at a constant temperature of 310 K determined at the gel-crystalline phase in previous works[23]. The Berendsen method was used to maintain the NPT ensemble, while bulk solvent and bilayers were controlled separately with a relaxation time of 0.25 ps; the gas atoms were coupled to the solvent phase. Semi-isotropic pressure control was employed. A time step leapfrog integrator was used every 2 fs, and the linear constraint solver (LINCS) algorithm was applied to preserve the bond lengths. The non-bonded pair list was updated every 10 steps with a cutoff of 1.0 nm. For the short-range van der Waals interactions, a cutoff distance of 1.0 nm was used. The long-range electrostatic interactions were treated by the particle mesh Ewald method, with a grid spacing of 0.12 nm; cubic interpolation was adopted. The volume compressibility was chosen to be 4.5×10^{-5} bar^{-1}. Data were collected every 2 ps. All simulation systems were energy minimized by the steepest descent method for 10^4 steps prior to submitting the data to a production run. Python 3.2.3 scripts were written for statistical data analysis, applying GROMACS analytical utilities on MD trajectories at $1ns^{-1}$ frequency, in order to enable sufficient sampling of statistically independent data.

Results and discussion

Starting the discussion with the pressure effects on biomolecules and lipids in particular, the issues to be addressed are (1) how sensitive are computation-based experiments on biological soft matter at extreme conditions, and (2) would the data provided by these methods be useful? Simple LJ liquids are the best examples of thorough exploration of simulations under a wide range of hydrostatic pressures. Pressure evaluation at the atomic level has been done by scaling the volume and hence the bond lengths by applying the normal Berendsen barostat for NPT ensembles, as has been described in the methods section[24]. The bond length is expressed by this means as a function of uniform hydrostatic pressure and a function of a scaling parameter that changes the attractive component of the LJ solvent-solute interaction[25,26]. The Berendsen weak coupling method does not correspond to any known statistical mechanical ensemble and may lead to artefacts in isolated molecules; however, it is common practice to apply Berendsen rescaling for relatively large biomolecules in explicit solvent, assuming that the approximation produces satisfactory data for statistically evaluated properties[27]. Simple LJ systems reveal many of the complex features observed experimentally for which the bond length changes are inferred by Raman peak shifts upon an applied uniform pressure in the 1 kbar range[28]. Accordingly, the DOPC bilayer density was evaluated in a simulation box at the same pressure range.

Lipid bilayer thickness and rate of gas diffusion

The average values for the densities of stacked DOPC atoms assigned as bilayer thickness profiles were sampled over every 1ns of 200 ns-long trajectories. Data for 1 and 1000 bar pressures are presented in Fig. 1A. The fluctuations of maximal gas densities peaking along 60ns of MD trajectories are shown in Fig. 1B, which also gives an estimate for the dynamics of gas penetration into the lipid membrane. In Fig. 1A, blue curves are assigned to pure DOPC bilayers at standard (continuous line) and extremely (broken line) hyperbaric conditions, which almost match those referring to the intact bilayer thickness of 4.0 nm (distance between highest density peaks)[54]. The bilayer at 1000 bar, however, demonstrates higher headgroup densities of 1100 v. 1000 kg m^{-3} under standard conditions. The membrane thickness parameters associated with noble gases, however, clearly show an expansion of the bilayer structure coupled with reduced maximal densities. Under the influence of anesthetic xenon and argon (black and green lines), the bilayer still maintains a precise lipid-solvent boundary; the density peaks, however, shift inward at the maximum simulated pressure.

It has been shown in previous experimental and computational works that inhaled noble gases accumulate *in vivo* in lipid bilayers[21,23,55,56]. Non-anesthetic neon under standard conditions demonstrates a very dissimilar boundary pattern (Fig. 1A, red continuous line). The complementary density data for carbon atoms of the DOPC choline group under Ne are also available in Supplementary Materials (S1A). The deformation of the lipid-solvent boundary by neon at low and moderate pressures (1 - 100

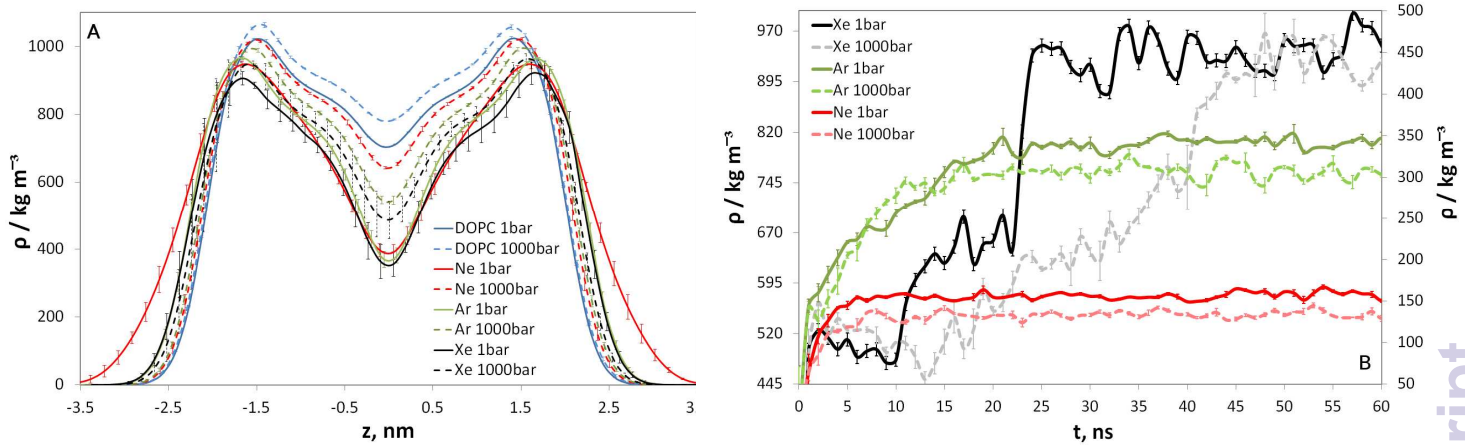

Figure 1. A: DOPC average density profiles are shown for intact DOPC (blue lines); Ne (red lines); Ar (green lines); Xe (black line) at 1 bar (continuous lines) v. 1000 bar (broken lines). B:The gas densities peak fluctuations v. simulation time are shown across the DOPC bilayer for Xe (black and grey) right scale, Ar (green) and Ne (red) left scale, at 1 (continuous lines) and 1000 bar (broken lines).

bar) is characterized by broad density peaks, and implies significant breakage of the lipids headgroup planar arrangement and development of a noisy, rough interface. This simulated phenomenon completely disappears as the pressure increases beyond 100 bar; the sharply pointed density peaks stabilize at separation distances of 4.0 nm - 4.2 nm.

Based on the density deviations, it may be possible to define two types of bilayer deformation. The noble gas atoms appear to inflate the bilayer owing to their concentration in the interlayer gap, which causes deformation and distortion of the ordinary membrane curvature. This type of deformation correlates directly with the gas' atom size and is most prominent for xenon: a density shift of almost 0.5 nm for each monolayer, compared with intact DOPC.

Hydrostatic pressure reduces such deformation, although the membrane remains inflated even at very high pressures. Argon's inflation pattern is very similar to that of xenon, with a density shift of 0.46 nm - 0.48 nm. The second type of packing disorder is evident with the small atoms of neon under low and intermediate pressures (this could be extrapolated to helium) and would be associated with the lipid-solvent boundary *per se* at the level of each monolayer. A possible explanation for the irregular boundary appearance of neon in the 1 - 100 bar pressure range, with its subsequent smoothing at higher HHP values, could be given, considering its higher velocity and therefore higher momentum impact per DOPC molecule, in this pressure range. The effect of gas atoms on lipids' undulations in the z-direction is discussed in detail below.

The initial inflation of the bilayer by xenon at standard conditions lasts up to 25 ns, while a rise in hydrostatic pressure increases this period up to 45 ns (Fig. 1B). Xenon penetration has a complex pattern characterized by initial gas accumulation close to lipid headgroups (1bar: 0-10ns; 1000bar: 0-12ns) with subsequent percolation within the bilayer gap. Argon, on the other hand, displays smooth logarithmical saturation at 15-20 ns disregarding the hydrostatic pressure applied. Neon, being highly penetrative at 1 bar, fills the bilayer gap in 5ns at 1bar, although its ability to inflate the bilayer at 1000 bar is significantly limited – the density profile is mostly similar to the native DOPC (Fig. 1A); it reaches maximal density within the bilayer gap within 8-10ns. DOPC bilayer density fluctuations at 1 v. 1000 bar on the 200ns timescale are shown in S1B. Also to be considered is the intrinsic limitation of simulation experiments – assuming a constant number of gas molecules in the box, resulting in reduced density in the bulk solution as the gas molecules diffuse into the bilayer; this is not the case in physiological experiments, whilst a continuous gas inflow would significantly affect gas dynamics at the bilayer vicinity, especially for xenon molecules, when excessive gas crowding in the headgroup region can be an influential parameter.

Water orientational properties and water-gas density distributions

The solvent density profile in the vicinity of lipids must clearly and directly depend on its unique orientational properties at the membrane boundary. The first rank order parameters of water (the average cosine of the angle between the water dipole and membrane normal) was found to be distance-dependent on membrane normal projection of DMPC bilayers by Lyubartsev *et al*.[29]. The strongest electrostatic field at the lipid-water interface was caused by the charges at the N and P groups, which in turn cause preferential orientation of water dipoles. The distorted orientation of water molecules obviously helps their penetration into bilayers, as was shown by X-ray scattering experiments[30]. Deep in the membrane interior, the velocities of water molecules can exceed even those in the bulk solvent, and they undergo large-scale fluctuations[31].

Water dipole cosine values are shown in Fig. 2A for Xe v. Ne saturated and native DOPC at 1 and 1000 bar. The effects of gases on bulk solvent are mediated by the lipid headgroup. Gases *per se* show little change, although Xe at 1 bar, 1000 bar and Ne at standard conditions present slightly lower cosine peaks at 1.5 nm - 2 nm, while the prolonged peak inherent to Ne could be attributed to an irregular boundary, as being a characteristic property of small non-immobilizers. The limited number of water molecules that slide into the bilayer gap are completely randomly orientated.

The effects of HHP on the bulk water phase have also been studied by Ohulkov *et al*.[32] Monte-Carlo (MC) trajectories in the 10 kbar pressure range have been produced to analyze the evolution of the parameters of the hydrogen-bonded network in liquid water under gradual compression. It has been suggested that an increase in the density of liquid water under compression is mainly achieved not by decreasing the nearest H-bonded neighbor distances, but rather by the increased packing efficiency of non-bonded neighbors, accompanied by some bending and weakening of the existing H-bonds[33,34].

Being only slightly distorted by HHP, the water structure evolves around the guest molecules that are trapped (enclathrated) inside H-bonded water cages with complex geometrical shapes[35,36]. Xe clathrates are thought to be thermodynamically more stable than Ar clathrates at high pressures and temperatures[37]. Neon apparently forms ice-based hydrate rather than classic clathrate cages at 10 -10^4 bar pressure ranges[38,39]. Although it is widely recognized that hydrates do not form at physiological conditions, the effect of noble gases on the lipid membrane-water interface as the first locus of general anesthetic effects might be significant[11,12]

The data (which are referenced to gas and water (SOL) density plots and presented in Fig. 2B) indicate gas accumulation within the central gap between the two monolayers, while Ne-saturated solvent at 1000 bar and at 1 bar are two asymptotic curves confining the limits of a bulk solvent distribution. Gas density peaks are also characterized by different pressure response, with Ne showing the highest peak reduction at 1000 bar. HHP does not significantly affect gas partitioning within bilayers, which is unlikely to be a cause for anesthesia reversal, as has already been stated by Griepernau *et al*.[57] Fatty acids in the lipid bilayer have been described as possible binding sites for general anesthetics[58]. The affinity of noble gases for the highly hydrophobic environment of biomolecular complexes is well supported by other experimental and molecular simulations works[13,21,23,55].

Given density data on mutual lipids and gas-water distributions, some conclusions can be made concerning the relevance of indirect mechanisms of anesthesia on IGN. Indirect mechanisms usually attributed to lateral pressure (LP) profiles[59] and LP fluctuations might be directly related to anesthetic mass density peaks within bilayers[60]. The moderate LP changes in DOPC saturated by xenon at standard conditions have been observed by Booker *et al*.[23], and could be entirely associated with assumed very high concentrations of gas atoms in the simulation box, and might possibly be complete artefacts. The gases lack explicit interfacial affinity, as in the -OH hydroxyl groups in alkanols, and are indeed unable to cause sharp LP profile change, measured in hundreds of bar in the range of a few nm[61]. Moreover, non-immobilizer Ne must disturb the LP profile as much as Xe does (with some shift on Z dimension, however), according to their similar DOPC density profiles at standard conditions, therefore an indirect mechanism looks questionable from this perspective.

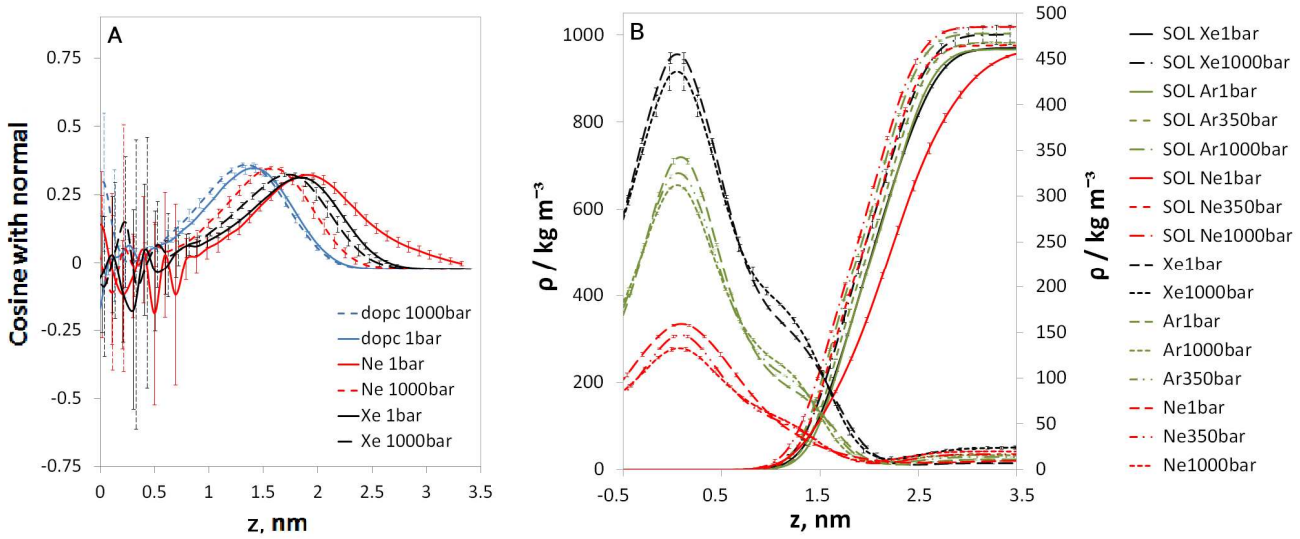

Figure 2. A: Cosines of water dipoles and bilayer surface normal angles are presented for Xe (black) and Ne (red) saturated bilayer v. intact DOPC (blue) at 1 bar (continuous lines) and 1000 bar (dotted lines). B: Density distributions across the simulation box are shown for Ne and Ar (right scale) and water and Xe (left scale) at 1, 350 and 1000 bar. Xe density value at 350 bar is not present as it is statistically insignificant. The density fluctuations are shown as error bars.

Area per lipid

The swelling of gas-saturated lipid membrane is another well-known phenomenon that is also observed on molecular simulation of a small fragment of it[23]. The area per lipid was estimated as a cross-sectional area of a simulation box (XY dimensions) sampled at the last 25 ns-long piece of each 200 ns trajectory divided by the number of DOPC molecules in each monolayer (144) Table 1).

The measured value refers to the intact DOPC area per lipid of 0.68 nm^2 at standard conditions (reported as 0.66 nm^2; ref.[47]). The value increases upon saturation with solvated gases, with xenon at low and moderate pressures having the largest impact. The HHP trends clearly represent bilayer compressibility at lateral dimensions and the effect of the distorted boundary at Ne in the 1 - 100 bar pressure range which is characterized by the lowest area-per-lipid values at standard conditions owing to planar arrangement distortion of DOPC molecules.

Lipid head group tilt angle

The average angle between the lipid dipole vector (P-N dipole vectors in the DOPC headgroups) and the bilayer normal defined as a tilt, was calculated in VMD[43] for all sampled trajectories, using a locally developed Tool Command Language script. The data in Table 2 for tilt angles and their standard deviations at 1 bar and 1000 bar depict no visible headgroup inclination; the stabilization is persistent around 90°. Significant deviation from this value has been reported for ionized solutions of monovalent salts, when the ions come in contact with charged phosphate groups[53]; neutral atoms of noble gases and HHP *per se* do not have this effect.

Lipid headgroup-water radial distribution functions

The effect of the level of hydration on lipids' fundamental properties, such as the order parameter and area per lipid, in turn affects the mechanical properties of the membrane and its phase behavior, as reported in numerous works[40,41]. In our analysis of lipid hydration, the explored limit of solvation was extended only up to O^{20} of glycerol group (Fig. 3).

Separated RDFs for water-lipid atom pairs of a headgroup were calculated with the Gromacs g_rdf tool and were used for estimating the water coordination numbers in the first coordination shell of DOPC atoms. The RDF gives the local density of species B around species A relative to the average density according to Formula 1:

Table 1. Area per lipid (nm^2)

P, bar	1	25	50	100	200	350	500	1000
DOPC	0.68	0.67	0.67	0.67	0.66	0.66	0.66	0.65
Ne	0.66	0.67	0.68	0.70	0.70	0.69	0.69	0.67
Ar	0.72	0.72	0.72	0.72	0.71	0.70	0.71	0.70
Xe	0.75	0.75	0.75	0.75	0.75	0.74	0.74	0.72

Table 2. Tilt angles and standard deviations presented at 1 bar and 1000 bar for intact DOPC bilayers and saturated with gases

P, bar	DOPC: Tilt, σ		Ne: Tilt, σ		Ar: Tilt, σ		Xe: Tilt, σ	
1	90.28	0.92	90.32	0.95	90.18	1.09	90.16	0.96
1000	89.56	1.03	89.46	0.88	89.91	1.21	90.07	0.89

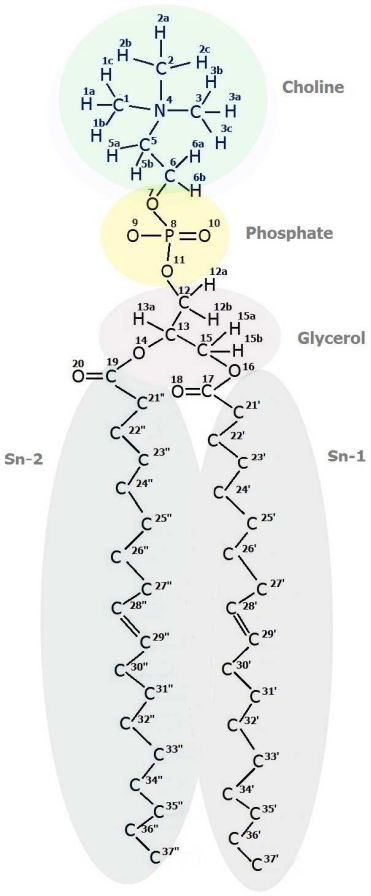

Figure 3. The diagram is a schematic presentation of the DOPC molecule and its functional groups. Atomic indexes for the radial distribution functions and order parameters are discussed in the text.

$$g_{ab}(r) == \frac{1}{N_A < \rho_B >} \sum_{i \in A}^{N_A} \sum_{j \in B}^{N_B} \frac{\delta(r_{ij} - r)}{4\pi r^2} \quad (1)$$

where N_A is the number of A particles, ρ_B is the density, and r the distance between the A and B species. The RDF is correlated with hydrostatic pressure according to the pressure equation (2) below. The pressure of a liquid is expressed as a function of the pair potential (u(r) is potential energy) and the pair correlation g(r)[42]:

$$P = \kappa_B T \frac{N}{V} - \frac{2\pi}{3} \rho^2 \int_0^\infty r^3 \frac{\partial u(r)}{\partial r} g(r) dr \quad (2)$$

To show the effect of noble gas atoms and hydrostatic pressure on the degree of solvation of a hydrophilic group, the appropriate RDF plots were sampled over all available 32 MD trajectories. The accepted water-headgroups' RDF integral values n_1 - the water coordination numbers were calculated in limits of r_0 – initial zero value of RDF; and r_1 – referring to the first minimum of g(r), as presented in Formula 3:

$$n_1 = 4\pi \int_{r_0}^{r_1} r^2 g(r) \rho dr \quad (3)$$

The integrals of solvent–DOPC atoms' RDF functions n_1^i (*i* = the atomic index of a DOPC molecule) are presented as one-dimensional curves referenced as gas solvation trajectories in Figure 4, for DOPC, Ne and Xe at 1bar and 1000 bar.

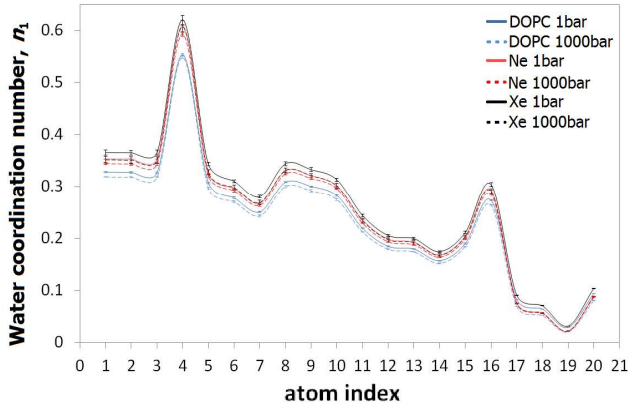

Figure 4 The solvent coordination number is shown for DOPC atoms of a headgroup for intact DOPC (blue line) v. bilayer saturated with Ne (red line) and Xe (black line) at 1 (continuous) and 1000 bar (broken line).

Two immediate conclusions can be drawn from the curve patterns in Figure 4. Firstly, the size of the gas atom has a clear solvation potency; xenon under standard conditions demonstrates the highest solvation potential, with n_1 normalized values of 1.15 – 1.20 relative to intact DOPC, while neon's solvation potential is quite moderate at 1.05 – 1.10. The comparatively minor differences distinguishable between solvation effects of noble gases v. intact bilayer enhance the questionability of indirect mechanisms, as mentioned above. Not only do the absolute values of the normalized functions differ, but also the slope of the solvation curves. The xenon curve shows a higher increase towards the hydrophobic carbons of acyl chains than the non-anesthetic neon curves. The glycerol region is characterized by reduced water density which does not provide clear resolution between gaseous effects. Additional plots dealing with relative RDF values are available in Supplementary Materials (S2). The peaks' prominence at oxygen atoms of phosphates and glycerol on integral RDF curves also correlates with the gas atom size; the bilayer curves for neon and especially pure DOPC exhibit a less prominent solvation pattern.

The second, and obvious, inference concerns the general desolvation effect of hydrostatic pressure as seen in Figure 5A-D, regarding the solvent RDFs of N^4, P^8, O^{16} and O^{18} atoms associated with the coordination number peaks in Figure 3. HHP evidently reduces solvation beyond statistically significant values at all presented plots, along with inherent water depletion from N^4 to O^{18}. At gas-mediated solvation plots at extremely high pressures such as 1000 bar, the shift of the curves towards lower values is accompanied by their flattening and rotation around the r_0 point. This finding might be explained by the opposing effects of HHP and the gas atoms within the coordination shells of headgroup atoms; the pressure rescaling generally reduces the volume and area per lipid, squeezing the membrane and expelling water dipoles. The anesthetic gas atoms make the membrane swell and thus increase solvation.

Lipid-gas radial distribution functions

The RDFs of gas-lipid atom pairs have been used for analyzing the gas phase layout within lipid bilayers. Assuming that the gas concentration gradient is normal to the bilayer plane, we ignored at this point possible lateral gas inhomogeneity being focused on pressure effects on oversaturated bilayers. Although the DOPC Sn_2 chain presents slightly higher values than Sn_1, as it is easier to reach higher gas gradients from $C^{21''}$ – $C^{37''}$ than for Sn_1, the RDF values at the two acyl chains (having similar slope patterns) were averaged and their integral value presented as shown in Figure 6 as gas coordination numbers for Ne and Xe at 1 and 1000 bar.

The undulations rate coefficients of DOPC molecules in the z-direction (D_z) for all explored systems at 1 bar v. 1000 bar (shown in the insert in Figure 6) have been evaluated at the non-equilibrium state, at the first 50ns of MD trajectories associated with initial bilayer inflation, based on the Einstein-Smoluchowski relationship of diffusivity and particle terminal velocity[62]. Hydrostatic pressure induces gas-atom redistribution within the compressed bilayer. For the heavier Xe atoms, however, it remains mostly within the limit of statistical insignificancy, being mostly overlapped in the region of the acyl chains. For Ne, the curve splitting is linear as the pressure increases, as the values of the integral RDFs go higher; at the same time, the Ne distribution pattern at standard conditions exhibits clear inconsistency which can be directly related to the DOPC's highest D_z value. Gases' drift velocities determined in the box show uniform distribution, disregarding the HHP value; their total diffusivity coefficients (D) are shown in Table 3. Given reduced Ne density in lipids intermolecular voids and considering Ne kinetics, the implication is that the highest momentum impact per DOPC molecule in the z-direction from a gas-filled cavity upon bulk solvent at standard conditions results in an irregular lipid boundary, as described in Figure 1A.

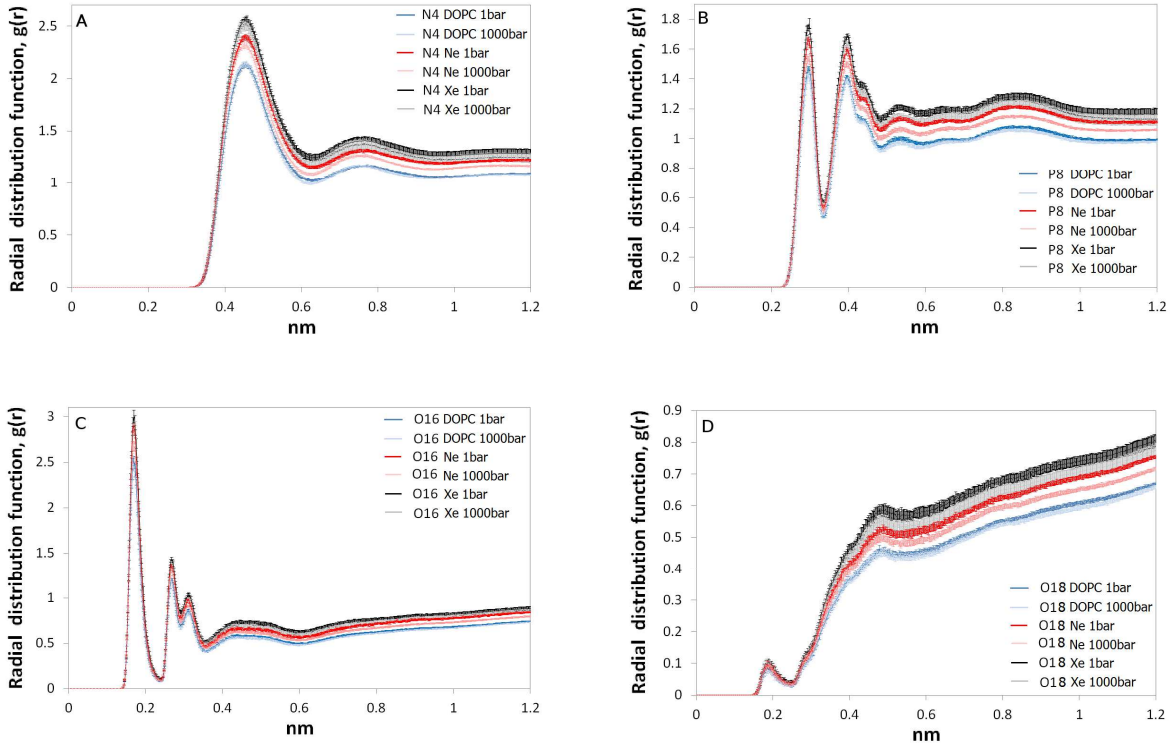

Figure 5. The radial distribution functions of water around (A) N^4, (B) P^8, (C) O^{16} and (D) O^{18} DOPC atoms are presented for intact DOPC (blue line) v. DOPC saturated with Ne (red line) and Xe (black line) at 1bar (dark error bars) and 1000 bars (light error bars).

The RDFs of gas-DOPC atoms N^4, P^8, O^{18} and C^{37} are shown in Figure 7. All the explored gases demonstrate similar patterns of distribution, but there are some quantitative differences between anesthetic Xe and non-anesthetic Ne, while Xe is characterized by higher statistical fluctuation. The hydrophilic solvated headgroup atoms constitute an explicit barrier for the gas atoms characterized by RDF values below unity. Their sieving effect on Xe atoms would be the most significant, thus altering diffusion into the bilayer. The small differences between the Xe RDF at 1 bar v. 1000 bar clearly show this phenomenon, considering also the decreasing lipid surface area (Table 1) which enhances gas retention in a solvated hydrophilic local environment (reduced normalized RDFs are also given in Supplementary Data S3). The hyper-polarizability of Xe atoms (which is not considered in the present simulation) may significantly enhance the lipid head obstruction *in vivo*, considering currently known Xe chemical shifts in lipid emulsions[44].

The neon RDFs present a clear pressure response which is most significant in the O^{16} region. The role of neon, and especially helium, as a simple pressure-conducting medium, has been discussed[45]. Regarding the relevance of our data for breathing a gas mixture such as Trimix (oxygen, helium and nitrogen) under hyperbaric conditions, our analysis suggests that helium can improve the diffusion of potentially narcotic nitrogen in the solvated headgroup region and thus neutralize its anesthetic effect. The intact lipid bilayer, however, reacts to any massive inclusion of alien atoms. The possible consequences of such distortions are discussed in the following sections.

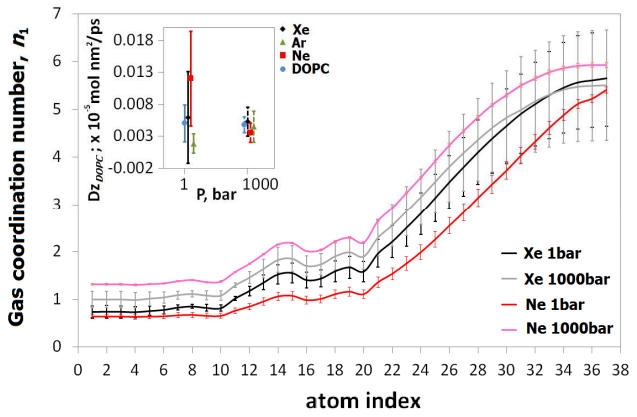

Figure 6. The coordination numbers are shown for gas molecules of DOPC atoms saturated with Ne at 1 bar (red line), 1000 bar (pink line), and Xe (black line) at 1 bar and 1000 bar (grey line). The DOPC undulations rate coefficients at the 0-50 ns MD range are shown in the insert for intact DOPC (blue), Ne (red), Ar (green), Xe (black) at 1bar (continuous) v. 1000 bar (broken line).

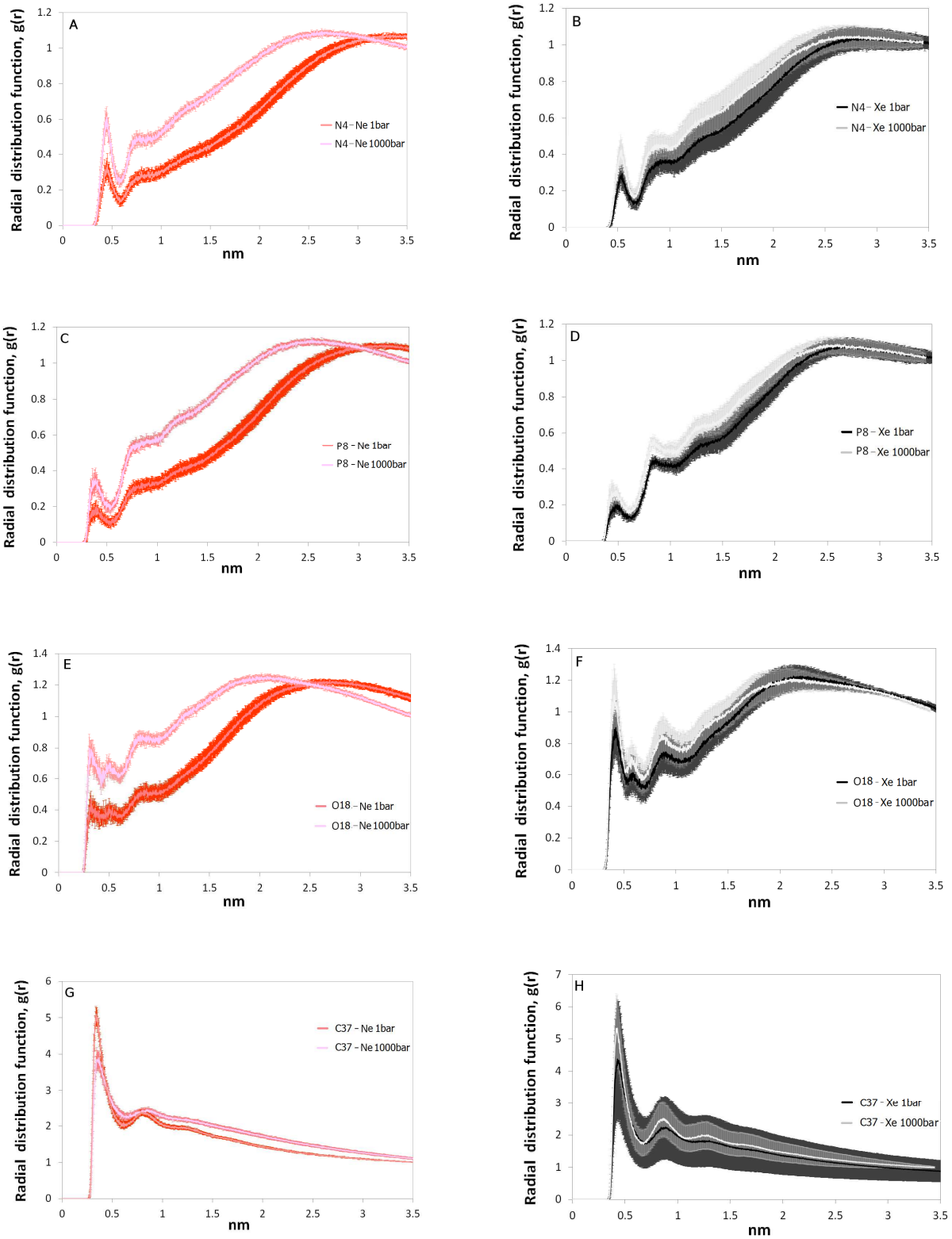

Figure 7. The radial distribution functions of Ne molecules around N^4 (A), P^8 (C), O^{18} (E) and O^{37} (G) DOPC atoms; and Xe around N^4 (B), P^8 (D),O^{18} (F) and O^{37} (H) DOPC atoms are presented at 1 bar (red error bars Ne, black error bars Xe) and 1000 bar (pink error bars Ne, grey error bars Xe).

Journal Name RSCPublishing

ARTICLE

Table 3. The diffusivity coefficients of three gases (*D*; mol nm^2/ps) sampled in the 0-50ns range of MD trajectories are presented at 1 and 1000 bar.

P, bar	*D,* Ne	σ	*D,* Ar	σ	*D,* Xe	σ
1	6.04E-04	4.31E-05	3.15E-04	3.05E-05	9.61E-05	5.18E-06
1000	6.10E-04	3.45E-05	3.04E-04	7.78E-06	9.59E-05	5.75E-06

Lipid order parameter

The deuterium lipid order parameters $Sn_{1,2}$ of the two carbon tails of the DOPC molecule (Figure 3) have been separately tested using the g_order Gromacs software under a wide range of conditions, and are presented as unique and average functions (Figure 8, A–C).The order parameter is derived from the quadrupole splitting of nuclear magnetic resonance (NMR) spectra, and is determined by selective deuteration of successive carbons of the acyl chains. At lipids' MD trajectories, the molecular order parameter can be estimated as[46]:

$$S_{ij} = \frac{1}{2}(3\cos\theta_i \cos\theta_j - \delta_{ij}) \quad (4)$$

where Θ_i is the angle between the *i*th molecular axis (*i,j*) and the bilayer normal. The C_nH bond vector used as the molecular axis S_{zz} yields the experimentally measured S_{CD} value. In the united atom models, such as that of Berger, the segmental vector connecting adjacent carbons in the acyl tail is taken as the molecular axis. The deuterium order parameter S_{CD} is described by the formulae below for saturated and unsaturated carbon tail atoms:

$$-S_{CD}^{sat} = \frac{2}{3}S_{xx} + \frac{1}{3}S_{yy} \quad (5)$$

and

$$-S_{CD}^{unsat} = \frac{1}{4}S_{zz} + \frac{3}{4}S_{yy} \pm \frac{\sqrt{3}}{2}S_{yz} \quad (6)$$

In a comparative analysis of the generalized AMBER and Berger force fields, Siu *et al.*[47] describe the differences between the results of deuterium NMR data for lipid acyl chains and the MD simulations using the Berger force field for DOPC bilayers. Their conclusion is derived from NMR results as well as from X-ray diffraction studies on the inequivalence of the chains close to the glycerol backbone. Disregarding the polar headgroup, it was concluded that the orientations at the beginning of the chains differ significantly, with chain Sn_1 being oriented perpendicularly, and chain Sn_2 parallel, to the bilayer surface, which is a general feature of phospholipids within membranes[48]. Berger lipids do not exactly reproduce this behavior, which makes conformational analysis practically impossible, but were largely chosen for the present research because of the calculation efficiency; however, the dissimilarity of Sn_1 and Sn_2 is in any event mentioned in our order parameter report.

The order parameter curves presented in Figure 8B reflect the normalization done using the curves for intact DOPC under standard conditions (Figure 8A) for discriminating between the different types of effects not distinguished at ordinary $Sn_{1,2}$ plots. The data presented are the average of normalized $<Sn_1>$ and $<Sn_2>$ (non-normalized curves available at Supplementary Data S4). Generally, the order parameter at the double-bond segments as the function of pressure is concave up as an effect of pressure increase; with all explored gases, however, it is clearly concave down, indicating this finding as a fundamental difference between anesthetic or gaseous and HHP effects at the level of lipid conformation. Different patterns of the curves' concavity determine opposite trends in the 30 – 37 C region; the patterns represent a steady increase at the intact DOPC molecule, while HHP pushes the curves down at the gas-saturated

bilayer. The highest pressure response shift is observed for Ne; under standard conditions, it goes below the unity curve in the 21 – 28 C region while, for Xe and Ar, the normalized curves for Sn_1 and Sn_2 are constantly above the 1 threshold line for all pressure ranges. The Sn_1 and Sn_2 chains are not completely identical; Sn_2 is more sensitive to all types of pressure reaction, but deviations within the

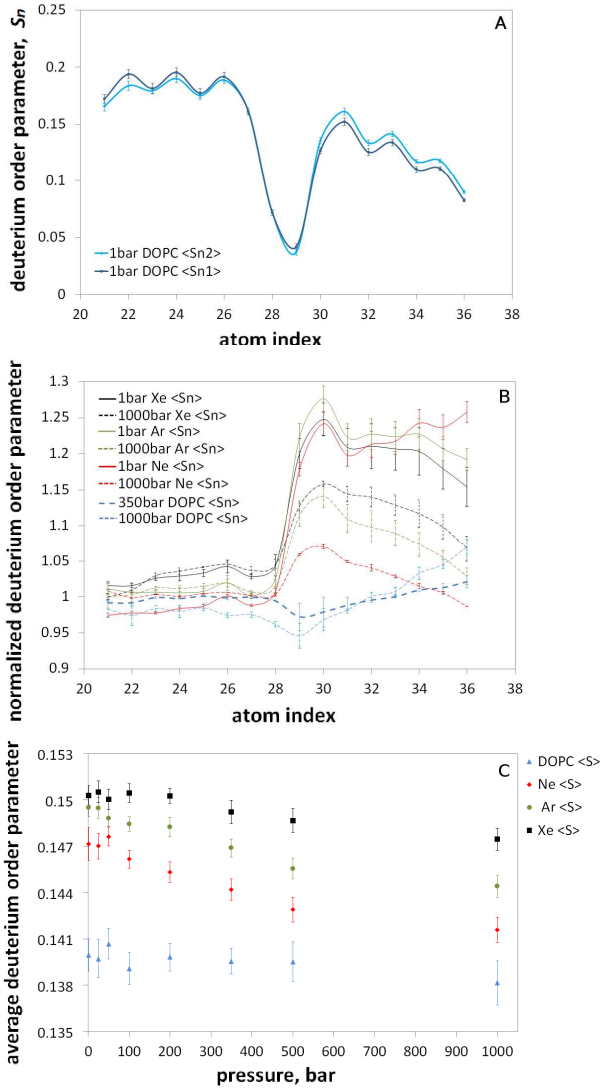

Figure 8. A: Order parameter curves of intact DOPC at standard conditions are shown for both acyl chains. B: Normalized order parameter curves averaged for Sn_1 and Sn_2 with different gases and pressure values shown; curves of intact DOPC at standard conditions are used as a reference. Opposite concavity of curves is clear for gases and HHP per se. *C: Average values for all curves presented. Incompressible intact DOPC is shown v. compressible gas inflated bilayers.*

2% – 8% range allow averaging of the order parameter values for both acyl chains (Figure 8C). The dots shown are within standard uncertainties, but the final pressure values for all three gases are distinct from the initial values beyond the error bars, while the average of the intact DOPC dots remains within the standard error deviation zone at the entire explored pressure range of 1000 bar. This observation could be described as the compressibility of the gas-inflated bilayer v. the notable incompressibility of the intact DOPC membrane.

Raman and infrared spectra of fully hydrated bilayers of DOPC are reported for increasing hydrostatic pressures up to 37 kbar[49]. Abrupt changes in the Raman spectrum of aqueous DOPC take place between 4.2 kbar and 5 kbar, which is beyond the scope of this study; however, the following analogy should be noted: the gases, acting synergistically, have the same effects as HHP, showing a significant increase in the ordering of the crystalline phase at least, for the highly hydrophobic C^{30} – C^{37} regions of acyl chains. A similar observation is true also for other hydrophobic substances such as cholesterol, which also significantly decreases the amplitude of the hydrocarbon chain motion, and the structure of the bilayer is predominantly ordered[50]. Well-known general anesthetics such as halothane, with high dipole moments, aggregate preferentially near the complex headgroup region and decrease lipid order parameters[51]. Consequently, the order parameter changes in highly hydrophobic regions have only marginal anesthetic effects, especially considering the fact that non-anesthetic neon has the highest ordering influence at 1 bar. A strong ordering effect by helium, for example, was described by Trudell *et al.*[52]; on the other hand, the importance of the different hydration potencies of the three gases tested is in agreement with the results of other works, and points to a hydrophilic head as the main focus for general anesthetic processes.

Neurophysiology of HHP effects and inert gas narcosis

The simulation of a small patch of lipid membrane with a simple non-polarizable force field is unable to reveal the entire complexity of anesthetic and high-pressure neurophysiological phenomena. However, it makes it possible to discriminate between the anesthetic gases Xe and Ar, the non-anesthetic Ne (alluding to He and He tremor at HHP), and HHP *per se,* and thus eventually to draw connections to the fundamental physiology of CNS. Based on the latest data available, gaseous general anesthesia could be described as a series of macromolecular events including sharp LP perturbation within the bilayer and inflation of highly hydrophobic cavities within the embedded transmembrane protein ion channel[13,59,64]. Water molecules play a key role in ionic conductivity, enabling ionic

passage through the channel, and should be considered explicitly in analysis of these events[65]. While it is unclear whether channel- or bilayer-determined occurrences are dominant in IGN, they clearly have a complementary role in the *final* processes at the biomolecular interface directly responsible for ionic channel functioning. Over-hydration owing to a decrease of sharp lateral pressure peaks is as possible as direct over-hydration owing to anesthetic gases diffusing through the channel's lumen into hydrophobic cavities, as similarly reported for ethanol trajectories[66]. The unnatural opening and over-hydration of the channel will end up with increased and uncontrollable ionic flow by analogy with channel mutants, where a hydrophobic central patch of the channel was modified and replaced with less hydrophobic moiety[67]. Not only polarizable large atoms of the noble gases but especially diatomic gases such as oxygen, nitrogen and hydrogen with induced dipoles, would impose the same effect as their concentration increases beyond the critical threshold along with HHP. The deep solvation trajectories of noble gases are clearly shown for the DOPC headgroup atoms, xenon appears to be the most powerful enhancer under standard conditions. While the squeezing effect of dynamic solvation forces on the radius of gyration of globular proteins has been reported[68], the conformational changes of transmembrane proteins are apparently opposite, considering their different packing order. The probability also exists that gas-biased hydration of a lumen does not involve significant protein structure perturbation, contrary to other general anesthetics (considering a reported moderate LP decrease[23]) and could be a dominant factor at IGN (Figure 9 (right sketch)). In this respect, Paulling's theory of gaseous anesthesia can be revised and Miller's hypothesis might be proven, if we consider distorted water molecules in the solvation shell of lipid headgroups.

Concerning the direct anesthetic effect on proteins and its reversal by HHP, some further observations can be made. Conformational changes at 20 bar in saturated with xenon ureate oxidase have been described by Colloc'h *et al.*[13] The flexible, highly hydrophobic cavities occupied by gas atoms that impose their volume expansion, correlated well with gas narcotic potency[69]. The most pertinent question that remains is how HHP neutralizes IGN. Yamamoto *et al*. describe pressure reversal as the jamming of xenon atoms in the hydrophilic headgroup region, which antagonizes the effects of xenon by suppressing its diffusion into the protein cavity[55]. Such a jamming indeed happens according to our data too, especially at extremely high pressures of around 1000 bar (Figures1,2B; 7B,D).

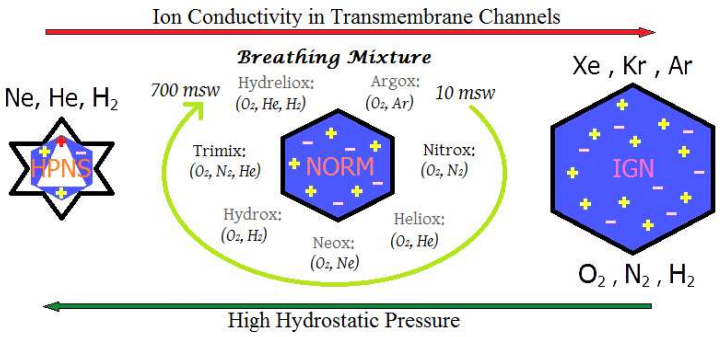

Figure 9. Schematic presentation of possible effects of gases and HHP on ionic conductivity via membrane-embedded channels and lumen hydration (blue color). Cations and anions are shown as plus and minus symbols; an adsorbed ion is shown in red. The list of breathing mixtures is given at the center according to their maximal operating depth (MOD), increasing clockwise.

However, we suggest a different interpretation of the pressure reversal, considering the fact that, at a 200 ns timescale, the maximum gas density was constantly associated with the gap between the two monolayers at all tested pressures. The 'critical volume' hypothesis seems to be the most appropriate, considering the evolution of the acyl chains' order parameter and their opposite concavity at gaseous saturation v. HHP increase[70]. By extrapolating the same types of conformational perturbations to flexible hydrophobic cavities of proteins, it could be concluded that HHP not only reduces the volume expanded by gases but also inverts configurational (geometrical) changes. Coupled with reduced biomolecular hydration, these changes would restore normal ionic flux through the channel (Figure 9, central sketch).

The next class of observations should relate to inert non-immobilizers such as Ne and He, and probably H_2, since their properties can be easily interpolated. In hyperbaric breathing mixtures, these gases act as diluents, suppressing the narcotic effects described above, and keep the transmembrane ion channel functioning normally, apparently by enhancing the narcotic gases' diffusion into and out of the bilayer and protein cavities, being often described as simple pressure transmitters into the bilayer[45,71]. Fig. 9 (center) presents the list of breathing mixtures according to their MOD, increasing clockwise, comprising heavy and light gaseous molecules. Ne and He do not inflate the bilayer as much as Xe and Ar do, but Ne's effect on bilayer integrity, especially in the 1 – 100 bar range associated with HPNS, is the most significant, as has been shown by our calculations, showing its effect on the DOPC undulations rate coefficient. Frank and Leib's work on the

cholesterol bilayer saturated with He at 1 – 210 bar reported no visible change in the neutron-scattering density profiles, even though cholesterol lacks a hydrophilic head such as that in DOPC[72]. However, the experimental data that have accumulated for almost 50 years provide strong evidence of neurological disorder under hyperbaric He, which can be described as enhanced excitability of the CNS[73,74].

The irregular lipid-water boundary shown in this study makes it possible to suggest a new hypothesis for He tremor at the atomic scale. Ne and He, being highly diffusive through biomolecular complexes, are unable to cause such configurational deformations in protein cavities as do anesthetics. However, the local momentum impact of these gases, filling protein cavities, exceed the impact of narcotic gases, considering their higher drift velocities, and results in spatial distortions, especially at the protein-solvent boundary. The influence of the rate of compression in the severity of HPNS could be also interpreted as the higher impact rate of the gas wave percolating into hydrophobic voids; it might additionally increase the amplitude of fluctuations in the gas-inflated molecular complexes. The distortions described possibly have long memory effects. Such distortions in transmembrane channels invariably affect the water lining, possibly breaking the water column in the lumen, which in turn causes reduced ion flow (Figure 9, left sketch). A similar type of distortion in ionic conductivity is reported in hydrophobic channel mutants; while the break in hydration of the ion would be expected to severely limit conductivity, as the ion is tied into the protein at the gate[75]. If the same types of ionic conductivity distortion owing to altered protein transcription processes take place in neurological disorders such as Parkinson's disease (PD)[63,86,87], which is characterized by motor dysfunctions similar to HPNS[88], xenon use under these clinical conditions might be considered[76]; furthermore, the knocking out of intact ionic channels by hyperbaric He can be proposed as a model for the etiology of PD. The neurological effects of ion channel blockers also support the hypothesis of ion flow reduction by non-immobilizers; for instance, reduction of low-threshold calcium currents in the channel model decreased the amplitude but increased the frequency of the simulated saccadic oscillations, in accordance with HPNS phenomena[77,78]. It should be borne in mind, however, that He might not necessarily lead to deactivation of the channel[79]; for as neon and helium can increase the cross-sectional area of a transmembrane channel, so can activation or deactivation depend on specific boundary conditions at the lumen in each case, while total CNS conditioning is apparently determined by the overall balance of deactivated/activated channels, i.e. the distortion/inflation balance.

Based on the preceding arguments, one can interpret the use of molecular hydrogen instead of nitrogen in a hydreliox breathing mixture for ultra-deep dives (owing to the comparable atom size of H and He, they can have the same diffusion paths). However, a slight dipole moment might be induced by the charged atoms from the hydrophilic envelope of biomolecules, which could affect molecular hydrogen retention and also create an anesthetic effect, additionally slowing down He diffusion into hydrophobic pockets. Molecular hydrogen very likely might have sedative and excitative effects simultaneously, which makes H_2 more a hallucinogen than an anesthetic[89]; but Zaltsman's experiments on mice at a remarkable 917 msw depth, with a hydrogen-containing breathing mixture, demonstrated that hydrogen indeed retains HPNS symptoms that manifest at greater pressures than with a helium-nitrogen mixture[80].

While anesthetic and non-anesthetic gases apparently differ in their neurological effects on transmembrane ionic flow, the influence of HHP *per se* still remains unclear. Simulations on proteins at HHP showed partial unfolding of their native 3D structure owing to loss of the hydrophobic effect as the solvent flux into the hydrophobic core increased[81]. Generally, the effect of HHP on biomolecules is complex; HHP favors electrostriction and promotes disruption of protein salt bridges, whereas hydration is opposed by pressure-induced reduction of cavity sizes and expulsion of water molecules[82], as described in our simulations. As an example of the physiological adaptation to HHP, long-term deep-sea inhabitants demonstrate the usage of organic osmolytes and ions to neutralize HHP by osmotic stress[83]. The HPNS main symptoms, for instance, were provoked equally in both He-O_2 and oxygenated fluorocarbon liquid dive groups comprised of dogs at 700-1000 msw depths[90], although channel deactivation by He might not be the same as by HHP and probably can occur at lesser P values. How does HHP affect the function of transmembrane ion channels in living organisms? Do organic osmolytes also help their stabilization? These questions remain to be answered in the future. Enhanced hydration flux owing to HHP is probable at some loci, as is hydrostatic squeezing dehydration at other subunits (explicit simulations of embedded proteins are needed for further comprehension). It is possible, however, that total liquid ventilation (LV)[84] combined with solvated conditional gaseous anesthetics such as Ar, N_2, H_2, and their mixtures at small concentrations, would significantly reduce

HPNS expression and can help to stabilize, to some extent, ion channel conformations against distorted water dynamics under HHP conditions – assuming even pressure values beyond 100 bar, which seems at the present to be absolutely not feasible concerning ventilation with noble gases. In this respect, there have recently been particularly promising advances in the field of clinical applications of LV technology coupled with high-frequency ventilation and/or extracorporeal CO_2 removal[85]; these have been approved by bioethics society and could lead to the next generation of life-support systems for underwater human activity at extreme depths.

Conclusions

The following conclusions can be made on the basis of our findings and within the limitations of the sampling methodology applied. Water, which is a highly ordered incompressible fluid, possesses a large spectrum of molecular orientation properties that can be changed over a wide range, particularly under the influence of hydrostatic pressure and at biomolecular interfaces. Considering the solvation shell as an integral part of the molecular structure, fluctuations in water density have been determined in the vicinity of DOPC headgroups. The noble gases demonstrate clear solvation potency correlated with the size of their specific atom. Hydrostatic pressure increase is associated with reduced solvent probability in the explored volume. The hydrophilic headgroup imposes a potential barrier on the noble gas atoms; the barrier is most prominent for anesthetic Xe at 1000 bar. Disregarding applied hydrostatic pressure values, the maximum density of solvated gases is always associated with the bilayer gap. Solvated gases inflate the bilayer. Xe presents the largest lipid head-head distance shift. Among the three gases tested, Ne shows the highest momentum impact at standard conditions on the DOPC bilayer, correlated with its higher drift velocity in the simulation box; however, pressure dependence of this correlation is not linear. The noisy (irregular) lipid-solvent boundary with a broken planar arrangement of DOPC headgroups has been observed at the Ne saturated bilayer in the 1 - 100 bar pressure range. Such packing disturbance disappears at higher pressure levels, while Ne partly leaves the bilayer gap and fills intermolecular voids. Disturbance of the molecular integrity of membrane-embedded complexes might be the reason for impaired ionic flow causing over-excitability of the CNS (which is also known as HPNS). Statistical analysis of the order parameter for DOPC acyl chains Sn_1 and Sn_1 shows the chains' compressibility upon saturation with gases. Nevertheless, the intact bilayer maintains the average order parameter within the limits of standard deviations across the entire 1 - 1000 bar pressure range. Considering that opposite concavities of normalized order parameter curves are saturated with gases or affected by HHP, one can presume the same reciprocity of conformational change in highly hydrophobic flexible cavities of transmembrane proteins occupied by the atoms of narcotic gases.

In summary, the observations of this study suggest the following conclusions: (1) noble gases are hostile to all compartments of a cell; they critically affect the cell's molecular machinery at all possible levels including, obviously and most drastically, the neurological signal transduction cascades; (2) HHP, on the other hand, is a natural condition for living organisms, with the vast majority of the Earth's biosphere living deep in the oceans, where indeed terrestrial life had its origins; (3) it is plausible to assume that the presence of intrinsic adaptive mechanisms to HHP is one of the most common characteristics of life, whereas there can be no adaptation against the pathological effects of hyperbaric gaseous environments; and (4) precise molecular mechanisms of HHP adaptation are unknown; in this regard, the use of modern computer technology in the thriving field of high-pressure biology is a powerful tool, providing new perspectives with the highest possible resolution in the study of these processes.

Acknowledgements

The authors thank Prof. Tibor Koritsanszky for fruitful discussions and his help in editing this paper. The authors acknowledge funding from the Office of Science in the U.S. Department of Energy; grant #DE-SC00005094.

References

1. Brubakk A, Neuman T, Bennett P, Elliott D. The Physiology and Medicine of Diving. 5th ed. Saunders Ltd, Philadelphia. 2002.
2. Sébert P. Comparative High Pressure Biology. Enfield, NH, USA. 2010.
3. Ruzicka J, Benes J, Bolek L, Markvartova V. Physiol Res. 2007;56: S39-S44.
4. Rostain JC, Lemaire C, Gardette-Chauffour MC, Doucet J, Naquet R J. Appl. Physiol. 1983, 54, 1063-1070.
5. D'Agostino D, Colomb D Jr, Dean J. J. Appl. Physiol. 2009, 106, 996-1003.
6. Sanders R, Ma D, Maze M. Br Med Bull. 2005, 71, 115-135.
7. Rostain JC, Gardette-Chauffour MC, Naquet R. J Appl Physiol. 1997, 83, 575-582.
8. Sato K, Naito Y, Kato A, et al. J Exp Biol. 2002, 205, 1189-1197.
9. Current Freediving World Records. 2013, http://www.aidainternational.org
10. Kylstra JA. Chest. 1965, 47(2), 157-159.
11. Urban B. Br J Anaesth. 2002, 89(1), 167-183.
12. Miller SA. Proc Natl Acad Sci USA. 1961, 47, 1515-1524.
13. Marassio G, Prange T, David H, et al. FASEB J. 2011, 25(7), 2266-2275.

14. Wlodarczyk A, McMillan P, Greenfield S. Chem Soc Rev. 2006, 35, 890-898.
15. Somero GN. Annu Rev Physiol. 1992, 54, 557-577.
16. Berger O. Biophys J. 1997, 72, 2002-2013.
17. Feller SE, MacKerell JA. J Phys Chem B. 2000, 104, 7510.
18. Davis JE, Patel S. J Phys Chem B. 2009, 113, 9183–9196
19. Griepernau B, Leis S, Schneider MF, Sikor M, SteppichD, Böckmann RA. Biochim Biophys Acta. 2007, 1768(11), 2899-913.
20. Verlet L, Weis JJ. Perturbation theory for the thermodynamic properties of simple liquids. Taylor & Francis. 1972
21. Stimson L, Vattulainen I, Rog T, Karttunen M. Cell Mol Biol Lett. 2005, Vol. 10, 563–569
22. HessB, Kutzner C, van der Spoel D, Lindahl E. J Chem Theory Comp. 2008, 4(3), 435–447
23. Booker R, Sum A. Biochimica et Biophysica Acta. 2013, 1828, 1347–1356
24. Berendsen HJC, Postma JPM, van Gunsteren WF, DiNola A, Haak JR. J Chem Phys. 1984, 81(8), 3684-90.
25. Everett JP,Faux DA. Physical Review B. 2008, 78, 054113
26. Gonçalves AS, Caffarena ER, Pascutti PG. J Braz Chem Soc. 2009, Vol. 20, No. 7, 1227-1234
27. Harvey S, Tan R, Cheatham TJ. Comput Chem. 1998, 19 (7), 726–740.
28. Hubel H, Faux DA, Jones RB, Dunstan DJ. J Chem Phys. 2006, 124, 204506
29. Ho1gberg CJ, Lyubartsev AP. J Phys Chem B. 2006, 110, 14326-14336
30. Mathai JC, Tristram-Nagle S, Nagle JF, Zeidel ML. J Gen Physiol. 2008, 131, 69–76.
31. Krylov NA, Pentkovsky VM, Efremov RG. ACS Nano. 2013, vol. 7 No. 10, 9428–9442
32. Kalinichev AG, Gorbaty YE, Okhulkov AV. J Mol Liq. 1999, 82 57-72
33. Bagchi K, Balasubramanian S,Klein ML. J Chem Phys. 1997, 107, 8561
34. Khusnutdinoff R, Mokshin A. J Non-Cryst Solids. 2011, V. 357, Issue 7, 1677–1684
35. Beauchamp B., C. R. Geoscience 2004, 336, 751–765
36. Walsh, M. R., Koh, C. A. Sloan, E. D. Sum, A. K. Wu, D. T. Science, 2009, 326, 1095
37. Sanloup, C. Mao, H. and Hemley, R. J., PNAS, 2002, vol. 99 no. 1 25–28
38. Loveday, J. S. Nelmes. R. J., Phys. Chem. Chem. Phys. 2008, 10, 937–950
39. Dyadin, Y.A. Aladko, E.Y. Manakov, A.Y. Zhurko, F.V. Mikina, T.V. Komarov V.Y. and Grachev, E.V., J. Struct. Chem., 1999, 40, 790–795.
40. Milhaud, J. Biochimica et Biophysica Acta, 2004, 1663, 19–51
41. DiSalvo, E. Lairion, F. Martini, F. Tymczyszyn, E. Frias, M. Almaleck, H. Gordillo, G., Biochimica et Biophysica Acta. 2008, 1778, 2655–2670
42. Bretonnet, J.-L. Thermodynamic Perturbation Theory of Simple Liquids. Pirajan, 2011, Ch 31.
43. Humphrey, W. Dalke, A. Schulten, K., J. Mol. Graph. 1996 , 14(1), 33-8, 27-8.
44. Sears, D. N. and Jameson, C. J., J. Chem. Phys. 2004, Vol 121, No 5
45. Winter, R. and Jeworrek, C., Soft Matter, 2009, 5, 3157–3173
46. Vanblitterswijk, W. Vanhoeven, R. Vandermeer, B., Biochimica et Biophysica Acta (BBA) - Biomembranes. 1981, Vol. 644, Issue 2, 323-332
47. Siu, S. Vácha, R. Jungwirth, P. and Böckmann. R. A., J. Chem. Phys. 2008, 128, 125103
48. Seelig, A. and Seelig, J. Biochim. Biophys. Acta, 1975, 406, 1
49. Wong, P. and Mantsch, H., Biophys. J., 1988, 54, 781-790
50. Hao, Y.H. Chen, J.W., J. Membrane Biol., 2001, 183, 85–92
51. Vemparala, S. Saiz, L. Eckenhoff, R. G. and Klein, M. L., Biophys. J., 2006, Vol. 91 2815–2825
52. Mastrangeio, C. J. Trude11, J. R. and Cohen. E.N., Life Sci. 1978, No. 3, Vol. 22, 239-244
53. Sachs, J. N. Nanda, H. Petrache, H. I. and Woolf. T. B., Biophys. J., 2004, Vol. 86 3772–3782
54. Pandit, S.A. Vasudevan, S. Chiu, S. W. Mashl, R. J. Jakobsson, E. and Scott, H. L. Biophys. J., 2004, Vol. 87 1092–1100
55. Yamamoto, E. Akimoto, T. Shimizu, H. Hirano, Y. Yasui, M. and Yasuoka, K., J. Phys. Chem. B 2012, 116, 8989−8995
56. Duhamel, G., Choquet, P., Leviel, J., Steibel, J., Lamalle, L., Julien, C., Kober, F., Grillon, E., Derouard, J., Decorps, M., Zeigler, A. and Constantinesco, A., 2000, Life Sci. 323 529-536.
57. Griepernau, B. Bockmann, R., Biophys. J. 2008, Vol. 95 5766–5778
58. Trudell, J. R. Goblin, D. D. and Eger, E. I., Anesth. Analg. 1998, 87, 411-8.
59. Cantor, R. S., Biophys. J. 2001, Vol. 80, 2284–2297
60. Darvas, M. Hoang, P. Picaud, S. Sega, M. and Jedlovszky, P., Phys. Chem. Chem. Phys., 2012, 14, 12956–12969
61. Terama, E. Samuli Ollila, O. H. Salonen, E. Rowat, A. Trandum, C. Westh, P. Patra, M. Karttunen, M. and Vattulainen. I., J. Phys. Chem. B. 2008, 112, 4131-4139
62. Philibert, J., Diffusion Fundamentals. 2006, 4, 6.1 - 6.19
63. Senthil Selvaraj, Yuyang Sun, John A Watt, Shouping Wang, Saobo Lei, Lutz Birnbaumer, Brij B Singh. J. Clin. Invest., 2012 Apr 2 , 122, 1354-67
64. Gullingsrud, J. Schulten, K., Biophys. J., 2004, Vol. 86, 3496–3509
65. Roux, B. Prod'hom, B. and Karplus, M., Biophys. J., 1995, Vol.68, 876-892
66. Murail, S. Wallner, B. Trudell, J. R. Bertaccini, E. and Lindahl, E., Biophys. J., 2011, Vol. 100, 1642–1650
67. Dong, H. Fiorin, G. Carnevale, V. Treptow, W. and Klein, M. L., PNAS, 2013, Vol. 110 no. 43, 17332–17337
68. Moskovitz, Y. Srebnik, S., Phys. Chem. Chem. Phys., 2012, 14 (22), 8013 – 8022
69. Seto, T. Isogai, H. Ozaki, M. Nosaka, S., Anesth. Analg. 2008, 107(4), 1223-8.
70. Miller, K.W. Paton, W.D. Smith, R. A. and Smith, E. B., Mol. Pharmacol., 1973, 9, 131.
71. Kato, M. Hayashi, R., 1999, 63(8), 1321-8.
72. Franks, N. P. and Lieb, W. R., Biophys. J., 1991, Vol. 60, 498-501
73. Talpalar, A. E. Grossman, Y., J. Neurophysiol., 2003, 90, 2106-14
74. Southan, A.P. and Wann, K.T., Eur. J. Neurosci., 1996, 8, 2571-2581
75. Kariev, A. M. Njau, P. and Green, M. E. Biophys. J., 2014, Vol. 106, 548–555
76. Xenon-based inhalable drug for treating or preventing induced dyskinesia. Patent US 20120213860 A1
77. Shaikh, A.G. Zee, D.S. Optican, L.M, Miura, K. Ramat, S. Leigh, R.J. Ann N Y Acad Sci. 2011,1233, 58-63
78. Guillemant, P. Ulmer, E. Freyss, G. Acta Oto-laryngol., 1995, Vol. 115, No. s520, 288-292
79. Aviner, B. Gradwohl, G. Mor Aviner, M. Levy, S. and Grossman, Y., FNCEL. 2014, Vol. 8 Art. 136 1.
80. Zaltsman, G.L., Hyperbaric epilepsy and narcosis. (English Translation No. JPRS 51714) USSR Academy of Science, Leningrad. 1968
81. Chara, O. RaúlGrigera, J. and McCarthy, A. N., J. Biol. Phys., 2007, 33, 515–522
82. Boonyaratanakornkit, B. B. Park, C. B. Clark, D. S., Biochimica et Biophysica Acta. 2002, 1595, 235-249
83. Yancey, P. H. Blake, W. R. and Conley, J., Comparative Biochemistry and Physiology Part A. 2002, 133, 667–676
84. Gabriel, J. L. Miller, T. F. Wolfson, M. R. Shaffer, T. H., ASAIO Jour., 1992, 42 (6), 968–973
85. Arazawa, D. T. Oh, H. Ye, S. Johnson, C. A. Woolley, J. R. Wagner, W. R. and Federspiel, W. J., J. Memb. Sci., 2012, 404-404, 25–31
86. Dworakowska B, Dołowy K. Ion channels-related diseases. Acta Biochim Pol. 2000; 47(3): 685-703.
87. Shieh C.-C., Coghlan M., Sullivan J. P., and Gopalakrishnan M., Pharmacol. Rev., 2000, 52, 557–593.
88. Filipova DT. Neurosci Behav Physiol. 1993 May-Jun;23(3):277-9.
89. Brauer RW (ed). Hydrogen as a Diving Gas. 33rd Undersea and Hyperbaric Medical Society Workshop. Bethesda: Undersea and Hyperbaric Medical Society; 1985.
90. Harris D.J., Coggin R.R., Roby J., Turner G, Bennett P.B., Undersea Biomed Res. 1985 Mar;12(1):1-24.